Primordial serpentinized crust on the early Earth

Bruno Reynard, Anne-Céline Ganzhorn, Nicolas Coltice

Title: Primordial serpentinized crust on the early Earth

Authors: Bruno Reynard[a], Anne-Céline Ganzhorn[a], Nicolas Coltice[b]

Affiliations:

[a]Université de Lyon, ENSL, UCBL, CNRS, LGL-TPE, F-69007 Lyon, France

[b]Laboratoire de Géologie, UMR8538, CNRS, Ecole Normale Supérieure, PSL Research University, 75005 Paris, France.

Corresponding author: Bruno Reynard bruno.reynard@ens-lyon.fr

Abstract:

Formation of a hydrated superficial layer early in the history of the Earth and Earth-like planets may occur by extensive serpentinization of mantle rocks by water, similar to that still active at present-day in slow-spreading oceanic plates. We investigated the lifetime of this buoyant and weak hydrated "crust" with 2D numerical simulations of mantle convection. Three regimes of preservation of the hydrated crust exist as a function of its thickness and buoyancy, both of which depend on the intensity of hydration. Firstly, an unlikely regime for the Earth is that where a thick buoyant crust (>100 km) can form a convective lid above the mantle. Secondly, a regime exists where weakly hydrated crust disappears through convection at a rate similar to the reference null hydration model. The lag time before which convection starts decreases with increasing thickness, decreasing the potential survival of the hydrated crust. Finally, a regime is found where rafts of highly hydrated crust of intermediate thickness are preserved at the surface. This regime is possible on the early Earth, and the survival time of the hydrated crust is proportional to its thickness. The present models indicate that a 50 km-thick fully serpentinized layer may have formed and survived over about 1 Gyr at the surface the early Earth, and could have favored the formation of the first differentiated felsic crust by partial melting.

Keywords: hydrated crust, serpentine, early Earth

1. Introduction

Hydration of the ultramafic to mafic rocks results in the formation of hydrous phyllosilicates like serpentine and chlorite. They play a major role in tectonic activity (Guillot et al., 2015) and subduction style (Gerya et al., 2008) because of their low yield strengths (Amiguet et al., 2012; Amiguet et al., 2014). A fully serpentinized crust is nearly as buoyant as continental crust but is reversibly transformed to anhydrous mantle rocks by dehydration in subduction (Ulmer and Trommsdorff, 1995), hence it has a limited lifetime once plate tectonics is active. Before the onset of plate tectonics and extensive formation of continental crust, an early Hadean hydrated ultramafic crust may have formed in a context of low-tectonic mobility (Boyet et al., 2003) and in the presence of a thick hydrosphere (Korenaga, 2007).

The early formation of a serpentinized crust in the Earth's history requires several conditions. A first condition is that water was available at the surface of the planet to form the serpentinized crust together with ultramafic to mafic rocks. The end of Earth accretion and differentiation is deemed to occur after the Moon-forming impact circa 4.4-4.5 Ga (Jacobson et al., 2014; Touboul et al., 2007), concomitant to major differentiation in the silicate Earth at 4.4 Ga as traced by the ^{146}Sm-^{142}Nd system (Carlson et al., 2019). Zircons from Jack Hills (Australia) ranging in age from 4.3 to 3.9 Ga were sourced from melts of weathered material that formed in the presence of water (Mojzsis et al., 2001; Wilde et al., 2001), suggesting water was present at the Earth's surface soon after the Moon-forming impact.

A second condition is that serpentine is stable, which imposes requirements on the superficial temperature gradient. At present time, serpentine is preserved at depths only in subduction zones (Reynard, 2013), as it destabilizes back to olivine and pyroxene at temperatures of about 900 K (Ulmer and Trommsdorff, 1995). It is marginally stable at the top of the mantle below oceanic or continental crust, except in slow-spreading oceans with core-complex structures in the crust (MacLeod et al., 2002). Archean plate tectonics in a

globally warmer Earth (van Hunen and van den Berg, 2008) favors thicker oceanic crust rather than serpentinization. The modes of cooling that are favorable for serpentinization over great depth assumed here are the heat-pipe (Moore and Webb, 2013) and squishy lid regimes (Lourenço et al., 2020) that were proposed to account for Hadean/Archean Earth conditions. Mass and heat flow through localized hot volcanic conduits and plutonic sills, while a slowly sinking lithosphere is maintained at temperatures below 900 K down to depth of up to ~200 km (Moore and Webb, 2013), allowing potential serpentinization and serpentine preservation down to these depths.

We explored through numerical models of thermo-chemical convection how such hydrated crust may have persisted at the surface of the early Earth in a context of convection onset.

2. Methods

We studied the stability of a hydrated layer (or primitive serpentinized crust) at the surface of a convective system. The hypotheses are that the hydrated layer has a lower density, lower viscosity and lower pseudo-plastic yield stress than mantle rocks, and that mantle dynamics is dominated by solid-state convection. Therefore we build a convection model with two distinct materials, being the mantle and hydrated rocks. The initial setup places the hydrated layer at the top of the system. We defined a depth of 300 km at which complete dehydration takes place, switching hydrated rocks to ambient mantle. Therefore sinking of hydrated rocks would lead to progressive vanishing of the initial layer. The purpose is to identify different regimes of stability by extracting time scales for survival/entrainment of this layer.

We model convection with the code StagYY in 2D spherical annulus geometry (Hernlund and Tackley, 2008), solving the following coupled non-dimensional equations:

$$\nabla \cdot v = 0 \tag{1}$$

$$\nabla \cdot \eta[\nabla v + (\nabla v)^T] - \nabla p = Ra(T + B_c C)e_r \tag{2}$$

$$\partial_t T + v \cdot \nabla T = \nabla^2 T + H \tag{3}$$

$$\partial_t C + v \cdot \nabla C = 0 \tag{4}$$

where v is the velocity, p the dynamic pressure, T the temperature, C the fraction of hydrated rocks (0 being only ambient mantle rocks and 1 being only hydrated rocks). The non-dimensional viscosity is η, H is the nondimensional heat production rate and Ra is the Rayleigh number based on the temperature drop between the base and the top of the model and B_c the buoyancy ratio defined below. We employ pseudo-plasticity where the viscosity is defined by:

$$\eta(T, p) = \eta_A(p) exp\left(\frac{E_a + pV_a}{T}\right) \tag{5}$$

$$\sigma_Y = \sigma_0 + d\sigma_Y' \tag{6}$$

$$\eta_Y = \frac{\sigma_Y}{2\dot{\epsilon}_{II}} \tag{7}$$

where η_A is the non-dimensional reference viscosity at pressure p, including a and step-wise 30-fold jump at 660 km, relevant to Earth (Ricard et al., 1993). E_a is the nondimensional activation energy, V_a is the nondimensional activation volume, σ_Y is the nondimensional yield stress (σ_0 being the surface value and σ_Y' its dependence on depth d), η_Y is the non-dimensional viscosity of yielded rocks and $\dot{\epsilon}_{II}$ the second invariant of the strain rate.

The tracer ratio method was used for composition (Tackley and King, 2003). We monitor the evolution of the composition to evaluate the survival timescale of the hydrated layer. A stable average composition means no recycling of the hydrated layer, and a composition of 0 everywhere means complete recycling and vanishing of the hydrated layer.

We use a reference parameterization for all convection computations (Table 1), varying only parameters of the hydrated layer. The reference setting is defined with a Rayleigh

number of 10^6 and a non-dimensional surface yield stress of 10^4. To obtain present-day Earth diagnostics given our formulation and choice of parameters, we would have to increase the Rayleigh number by one order of magnitude (Arnould et al., 2018). Working at lower Ra is easier to explore the parameter space. To transpose our results to dimensional values and Earth's convective vigor, we scale time so it can be compared to present-day Earth time. We assume that the non-dimensional time-averaged root-mean-square velocity at the surface of the reference model (no hydrated layer) at statistical steady state corresponds to that of the present-day Earth, being 3.9 cm y^{-1}. We call the transit time the time it takes a particle to travel a distance equal to the depth of the mantle at the rms surface velocity (with the value above for the Earth, it corresponds to 75 Myr). This classical choice of scaling gives a reference, but is by no means a precise extrapolation because for a younger Earth, the surface velocity is unknown.

The initial thermal condition corresponds to a 1D geotherm built from running the convection setup without the hydrated layer, where plate-like tectonic regime emerges and is sustained when the thermal statistically steady state is reached. The initial condition is therefore gravitationally unstable and destabilizes by recycling the surface boundary layer. A lateral harmonic perturbation is introduced to initiate the process.

Over this initial purely thermal setting we superimpose a hydrated layer. We study the efficiency of its recycling as a function of its density and thickness. We explore the role of material properties of hydrated rocks, having lower density and softer rheology than the ambient mantle. For the hydrated layer, we use a reference η_A and σ_Y 10 times lower than those of ambient mantle (Fig. 1). The hydrated layer is viscous close to the surface because it is cold, except in areas where the maximum stress is reached and shear zones may develop. The buoyancy number of the hydrated crust B_c is defined as $\Delta\rho_c / \Delta\rho_T$, where $\Delta\rho_c$ and $\Delta\rho_T$ are the density contrasts between hydrated layer and ambient mantle, and between the hottest and

coldest ambient mantle, respectively. B_c was set to 0, -0.034, -0.17, -1.7 and -3.4, corresponding for Earth to dimensional values of the density of the hydrated "crust" of 4400, 4355, 4310, 3510 and 2620 kg m^{-3}. The latter value is the nominal value of serpentine density in the high temperature antigorite form (Hilairet et al., 2006), for which the density jump with the incompressible mantle of average density of 4400 kg m^{-3} is 1780 kg m^{-3}, about twice the actual density jump between serpentine and dry peridotite. Models with this density jump are therefore likely unrealistic but were nonetheless performed to explore the stability of the convection regimes.

"Hydration rate" is defined as 100% for this extreme case, and would take values of 50, 5 and 1% for decreasing values of B_c. Models with half this density jump (B_c = -1.7) correspond to realistic values for a fully serpentinized upper layer. Models with B_c = -0.034, and -0.17 would represent a density jump if the crust is partially serpentinized to 2 and 10 %, respectively, for examples along deep discrete fractures such as those generated by thermal cracking (Korenaga, 2007). Thus serpentinization is more useful for the discussion, and is twice the "hydration rate" defined above. Serpentine contains about 12 wt% H_2O, from which the average water concentration in the simulation is obtained.

The thickness of the hydrated layer was set to 10, 50, 100 and 200 km (0.0034, 0.017, 0.034 and 0.068 in non-dimensional values). Calculations are named by the series of numbers indicating starting dimensional parameters as thickness (km)-hydration rate-simulation number (Fig. 2, Table 2).

3. Results

We monitored the decrease of the fraction of hydrated material in the system. Two reference solutions of entrainment are calculated before exploring the role of hydrated rocks material properties. These solutions correspond to the entrainment of a layer having the same

157 material properties as the ambient mantle, solutions Ref-1 and Ref-2 having 50 and a 200 km-
158 thick layers, respectively (Fig. 2a). The flow is identical in the two reference solutions, and
159 the top layer is quickly recycled by cold downwellings. The first subduction-like downwelling
160 (*i.e.* asymmetric to one-sided, continuous and stiff) initiates after about three transit times.
161 The 50 km-thick layer disappears within less than the duration of one transit time. In Ref-1,
162 small-scale convection or hot flow near the upper thermal boundary erodes slightly the deeper
163 "crust" before full model convection initiation (Fig. 2a). Recycling follows an exponential
164 decay with characteristic recycling half-life τ of less than 10 Myr, about one order of
165 magnitude lower than the transit time (Table 2).

166 Numerical solutions with a hydrated layer display three distinct regimes of hydrated
167 crust preservation depending on its initial thickness and density defined by the degree of
168 serpentinization (Figs. 2 and 3).

169 Regime I is observed for small density jumps between crust and mantle (2-10 %
170 serpentinization), where numerical solutions show a similar behavior to the reference
171 solutions (Fig. 2b). Temperature and viscosity fields show hot upwellings reaching the
172 surface, and cold downwellings penetrating the mantle that set up the global scale convection.
173 In that regime, the hydrated layer is entrained as a passive layer in the global flow pattern
174 because the integrated buoyancy of the top boundary layer is negative at all times. Once
175 downwelling initiates, the exponential decay time (τ~10-15 Myr) is similar to that of the
176 reference models, one order of magnitude lower than the transit time. For small thickness
177 (<50 km) of the hydrated crust, downwelling initiation occurs after about three transit times
178 (~200 Myr). Above 50 km thickness, downwelling initiates even faster because the hydrated
179 layer is weaker than the ambient mantle, favoring yielding and forming weaker slabs that sink
180 with less resistance.

Regime II is a domain corresponding to large hydration degree (50-100%) where the hydrated crust is slowly recycled (Table 2, Fig. 2c). The time of total disappearance of the hydrated layer is longer than the overturn time in reference calculations. Some calculations do not show complete recycling of the layer even after statistical steady state is reached. This dynamic regime is sustained because the hydrated layer brings the surface boundary layer close to neutral buoyancy. Temperature and viscosity fields show hot upwellings reaching the surface and cold downwellings penetrating the mantle (Fig. 2c). Where hot upwellings reach the surface, the hydrated layer yields, thins and stretches, ultimately forming buoyant rafts that drift. Above downwellings, the hydrated layer thickens and its base flows down into the mantle dragged by temporary flat and cold asymmetric slabs. Regime II corresponds to fully serpentinized crust of small to moderate thickness (Fig. 3), buoyant enough to cause recycling rate to be close to linear rather than exponential behavior of regime I, progressing at slower and regular pace. The constant flux of recycling does not depend on the volume of hydrated material that remains at the surface, and the entrainment characteristic time of hydrated crust τ is proportional to the percentage of hydration (Fig. 4). It means that in this regime, flat and cold downwellings erode regularly the hydrated material but do not entrain the full layer in subduction. Numerical solutions in which the rheology of the hydrated layer is identical to that of ambient mantle present the same characteristics as the solution with a viscosity contrast of 0.1, showing that the occurrence of regime II is controlled to first order by buoyancy, not by rheological contrast.

Two solutions fall in a third regime that displays no recycling even after statistical steady state is reached (Table 2, Fig. 2d). The corresponding parameter subspace is that of thick ($\geq$ 100 km) and extremely buoyant hydrated layer (100% hydration), imposing a stagnant lid tectonic regime with convective deformation within the hydrated layer decoupled from the convection within the ambient mantle. The transition between the mixing regimes

(Regime I and II) and the stable layer regime for a light surficial layer (Regime III) is symmetrical to the one observed in convection with a dense basal layer (Le Bars and Davaille, 2004). Regime III is unlikely on any terrestrial planet because of the excessive density contrast between hydrated crust and mantle.

4. Discussion and conclusions

Mantle convection models including a serpentinized primordial crust show the existence of 3 regimes of mixing/stability of such a light layer: Regime I being rapid exponential vanishing for low hydration degree, Regime II slow linear vanishing for efficient hydration over a moderate thickness, and Regime III survival for excessively light and thick crust.

Current estimates of the water content of the Earth (Marty, 2012; Piani et al., 2020) lie between 1 and 10 oceanic masses, corresponding to 350-3500 ppm in the bulk silicate Earth and to a 6.5-55 km-thick serpentine layer (12 wt% H_2O). Thus a primordial fully serpentinized crust may have reached about 50 km on the early Earth, and regime II was possible. A 50-km thick serpentine crust may have survived over several overturns (corresponding here to ~1 Gyr, Fig. 4). Such a thick serpentinized crust provides the ideal context of formation of a differentiated felsic crust at shallow depths (Borisova et al., 2021) over the first few hundred millions of the Earth history. Coexistence of TTG-type felsic crust and serpentinized ultramafic rocks would account for geochemical evidence for both 4.3 Ga differentiated crust recycling in Hadean Jack Hills zircons (Blichert-Toft and Albarède, 2008), and survival time of 1 Gy of a 50-km thick serpentinized crust for direct formation of the 4 Ga Acasta gneiss complex rocks from near surface ultramafic-mafic rocks (Reimink et al., 2016).

The present models could be improved since the setup was simplified in order to pinpoint physical behavior and for computational cost considerations. Firstly, the models are

2D, not accounting for 3D features like toroidal flow or cylindrical plumes. However the defined regimes are based on average properties that are usually similar in 2D and 3D convective systems. The Boussinesq approximation neglects the compressibility of rocks and the effects of phase changes. Since the explored regimes of recycling occur mostly in the upper mantle, the results should arguably not be strongly affected. Due to calculation time, the convective vigor of our models is lower than what is expected for the Earth. Scaling was thus based on surface velocities and characteristic transit/overturn times. Using the scaling of convective velocities with $Ra^{2/3}$, our results could be extended to cover ranges of young Earth-like values, potentially reducing the stability dimensional times by a factor of 3-10. However, models of a hot planet with large magma extraction show that the scaling of convection velocities with Ra does not hold, velocities remaining stable instead (Xie and Tackley, 2004). Exploring hydrated crust evolution with melt abundant mantle convection model and continent formation would be the next step to make.

Acknowledgments: This work was supported by grants to BR through the PNP-INSU program, and through LABEX Lyon Institute of Origins (ANR-10-LABX-0066) of the Université de Lyon within the program "Investissements d'Avenir" (ANR-11-IDEX-0007) of the French government operated by the National Research Agency (ANR). Thoughtful comments from an anonymous reviewer helped improve the manuscript.

References

Amiguet, E., Reynard, B., Caracas, R., Van de Moortèle, B., Hilairet, N., et al., 2012. Creep of phyllosilicates at the onset of plate tectonics. Earth and Planetary Science Letters 345-348, 142-150, 10.1016/j.epsl.2012.06.033.

Amiguet, E., van de Moortèle, B., Cordier, P., Hilairet, N., Reynard, B., 2014. Deformation mechanisms and rheology of serpentines in experiments and in nature. Journal of Geophysical Research 119, doi:10.1002/2013JB010791, doi:10.1002/2013JB010791.

Arnould, M., Coltice, N., Flament, N., Seigneur, V., Müller, R., 2018. On the scales of dynamic topography in whole-mantle convection models. Geochemistry, Geophysics, Geosystems 19, 3140-3163.

Blichert-Toft, J., Albarède, F., 2008. Hafnium isotopes in Jack Hills zircons and the formation of the Hadean crust. Earth and Planetary Science Letters 265, 686-702, 10.1016/j.epsl.2007.10.054.

Borisova, A.Y., Zagrtdenov, N.R., Toplis, M.J., Bohrson, W.A., Nédélec, A., et al., 2021. Hydrated Peridotite – Basaltic Melt Interaction Part I: Planetary Felsic Crust Formation at Shallow Depth. Frontiers in Earth Science 9, 10.3389/feart.2021.640464.

Boyet, M., Blichert-Toft, J., Rosing, M., Storey, M., Télouk, P., et al., 2003. 142Nd evidence for early Earth differentiation. Earth and Planetary Science Letters 214, 427-442, https://doi.org/10.1016/S0012-821X(03)00423-0.

Carlson, R.W., Garçon, M., O'Neil, J., Reimink, J., Rizo, H., 2019. The nature of Earth's first crust. Chemical Geology 530, 119321, https://doi.org/10.1016/j.chemgeo.2019.119321.

Gerya, T.V., Connolly, J.A.D., Yuen, D.A., 2008. Why is terrestrial subduction one-sided? Geology 36, 43-46, 10.1130/G24060A.1.

Guillot, S., Schwartz, S., Reynard, B., Agard, P., Prigent, C., 2015. Tectonic significance of serpentinites. Tectonophysics 646, 1-19, http://dx.doi.org/10.1016/j.tecto.2015.01.020.

Hernlund, J.W., Tackley, P.J., 2008. Modeling mantle convection in the spherical annulus. Physics of the Earth and Planetary Interiors 171, 48-54.

Hilairet, N., Daniel, I., Reynard, B., 2006. P-V Equations of State and the relative stabilities of serpentine varieties. Physics and Chemistry of Minerals 33, 629-637.

Jacobson, S.A., Morbidelli, A., Raymond, S.N., O'Brien, D.P., Walsh, K.J., et al., 2014. Highly siderophile elements in Earth's mantle as a clock for the Moon-forming impact. Nature 508, 84-87, 10.1038/nature13172.

Korenaga, J., 2007. Thermal cracking and the deep hydration of oceanic lithosphere: A key to the generation of plate tectonics? Journal of Geophysical Research: Solid Earth 112, https://doi.org/10.1029/2006JB004502.

Le Bars, M., Davaille, A., 2004. Whole layer convection in a heterogeneous planetary mantle. Journal of Geophysical Research: Solid Earth 109, https://doi.org/10.1029/2003JB002617.

Lourenço, D.L., Rozel, A.B., Ballmer, M.D., Tackley, P.J., 2020. Plutonic-Squishy Lid: A New Global Tectonic Regime Generated by Intrusive Magmatism on Earth-Like Planets. Geochemistry, Geophysics, Geosystems 21, e2019GC008756, https://doi.org/10.1029/2019GC008756.

MacLeod, C.J., Escartín, J., Banerji, D., Banks, G.J., Gleeson, M., et al., 2002. Direct geological evidence for oceanic detachment faulting: The Mid-Atlantic Ridge, 15°45′N. Geology 30, 879-882, 10.1130/0091-7613(2002)030<0879:DGEFOD>2.0.CO;2.

Marty, B., 2012. The origins and concentrations of water, carbon, nitrogen and noble gases on Earth. Earth and Planetary Science Letters 313-314, 56-66, https://doi.org/10.1016/j.epsl.2011.10.040.

Mojzsis, S.J., Harrison, T.M., Pidgeon, R.T., 2001. Oxygen-isotope evidence from ancient zircons for liquid water at the Earth's surface 4,300 Myr ago. Nature 409, 178-181, 10.1038/35051557.
Moore, W.B., Webb, A.A.G., 2013. Heat-pipe Earth. Nature 501, 501-505, 10.1038/nature12473.
Piani, L., Marrocchi, Y., Rigaudier, T., Vacher Lionel, G., Thomassin, D., et al., 2020. Earth's water may have been inherited from material similar to enstatite chondrite meteorites. Science 369, 1110-1113, 10.1126/science.aba1948.
Reimink, J.R., Davies, J.H.F.L., Chacko, T., Stern, R.A., Heaman, L.M., et al., 2016. No evidence for Hadean continental crust within Earth's oldest evolved rock unit. Nature Geoscience 9, 777-780, 10.1038/ngeo2786.
Reynard, B., 2013. Serpentine in active subduction zones. Lithos 178, 171-185, 10.1016/j.lithos.2012.10.012.
Ricard, Y., Richards, M., Lithgow-Bertelloni, C., Le Stunff, Y., 1993. A geodynamic model of mantle density heterogeneity. Journal of Geophysical Research: Solid Earth 98, 21895-21909.
Tackley, P.J., King, S.D., 2003. Testing the tracer ratio method for modeling active compositional fields in mantle convection simulations. Geochemistry, Geophysics, Geosystems 4.
Touboul, M., Kleine, T., Bourdon, B., Palme, H., Wieler, R., 2007. Late formation and prolonged differentiation of the Moon inferred from W isotopes in lunar metals. Nature 450, 1206-1209, 10.1038/nature06428.
Ulmer, P., Trommsdorff, V., 1995. Serpentine Stability to Mantle Depths and Subduction-Related Magmatism. Science 268, 858-861, 10.1126/science.268.5212.858.
van Hunen, J., van den Berg, A.P., 2008. Plate tectonics on the early Earth: Limitations imposed by strength and buoyancy of subducted lithosphere. Lithos 103, 217-235, 10.1016/j.lithos.2007.09.016.
Wilde, S.A., Valley, J.W., Peck, W.H., Graham, C.M., 2001. Evidence from detrital zircons for the existence of continental crust and oceans on the Earth 4.4 Gyr ago. Nature 409, 175-178, 10.1038/35051550.
Xie, S., Tackley, P.J., 2004. Evolution of U-Pb and Sm-Nd systems in numerical models of mantle convection and plate tectonics. Journal of Geophysical Research: Solid Earth 109, https://doi.org/10.1029/2004JB003176.

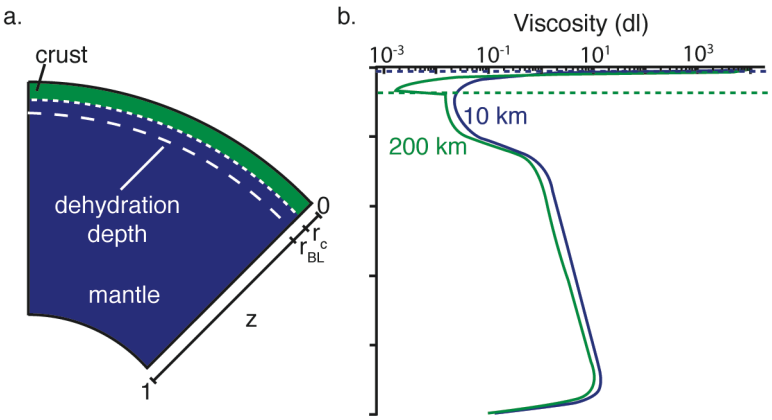

335

336 Figure 1: Initial set up. a. Schematic representation of the spherical annulus geometry with
337 two layers and definition of the different thicknesses. z is the depth of the mantle; r_c is the
338 hydrated layer thickness; r_{BL} is the thickness of the top thermal boundary layer (BL). b.
339 Viscosity profile for a fully hydrated crust thickness of 200 km and 10 km are compared. dl:
340 dimensionless.

341

342

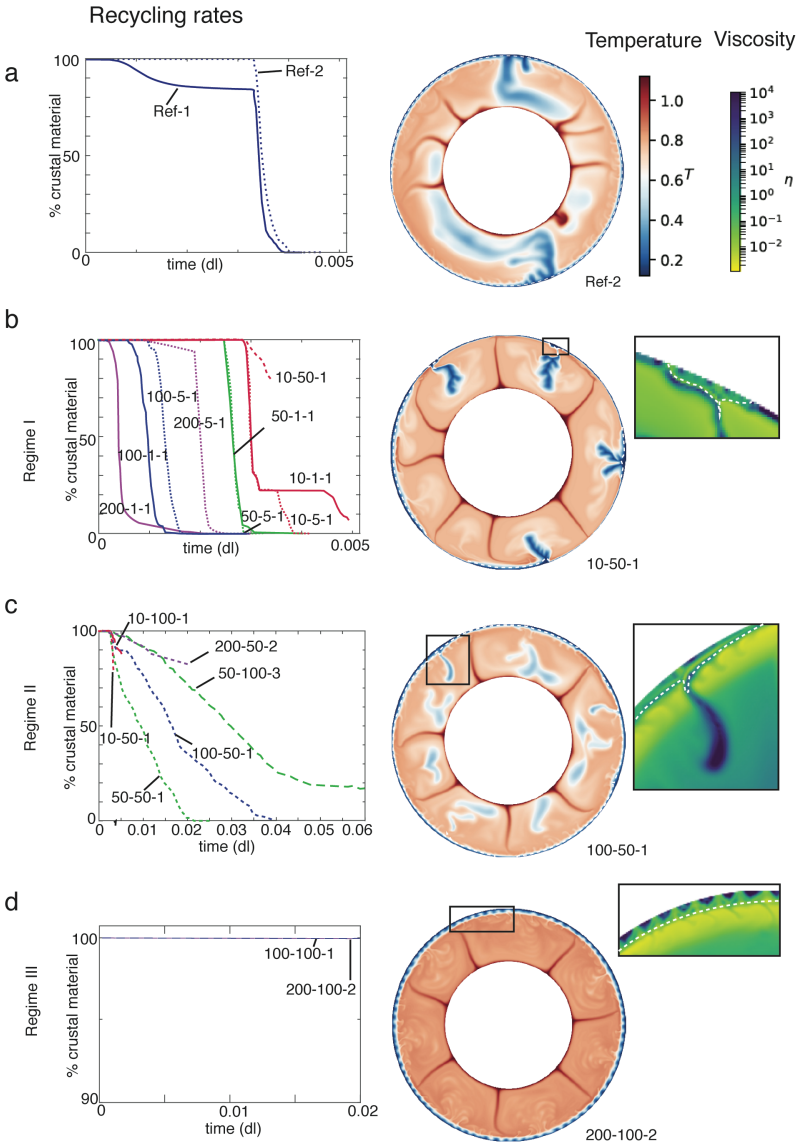

Figure 2: Characteristic recycling rates and flow patterns of the reference solutions (a) and of the three regimes of recycling/preservation of the hydrated layer (b,c,d). Surface recycling is similar in both simulations where the passive markers of "crustal" material have the same properties as the mantle. A dimensionless time of 0.001 corresponds to ~75 Myr for present Earth conditions, and the characteristic overturn time is ~300 Myr. Temperature snapshots are shown after downwelling/subduction initiation. Viscosity at the top of the mantle is shown for selected areas to illustrate tectonic features of the three regimes with hydrated crust. Temperature fields were obtained for two reference models with markers implemented over the first 200 km (Ref-1) and over the first 50 km (Ref-2).

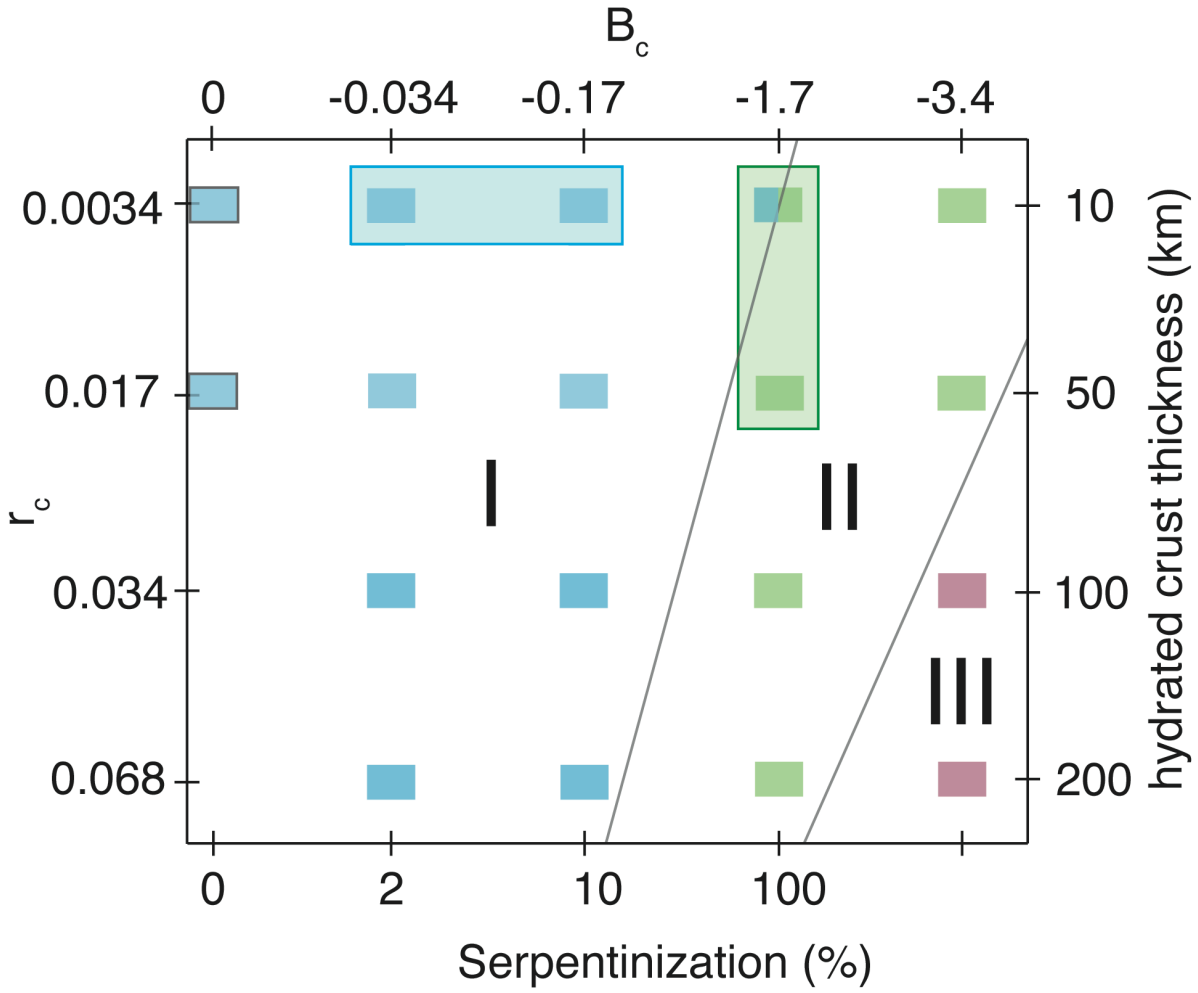

353

354 Figure 3: Crust recycling regimes as a function of the crust thickness and buoyancy contrast
355 (r_c: dimensionless crust thickness. B_c: dimensionless buoyancy number of the crust). Regime I
356 (blue) groups numerical simulations that share the same characteristics as the reference
357 simulations with fast disappearance of the crust duet to direct entrainment by downwelling,
358 regime II (green) simulations where hydrate crust is eroded by downwelling and its
359 disappearance time depends on crust thickness, and regime III (pink) where the hydrated crust
360 is preserved. Typical thickness and degree of serpentinization are reported for present-day
361 Earth (blue box) and Early Earth (green box). Note that the density contrast for the last
362 column is not compatible with known degrees of serpentinization (see text).

363

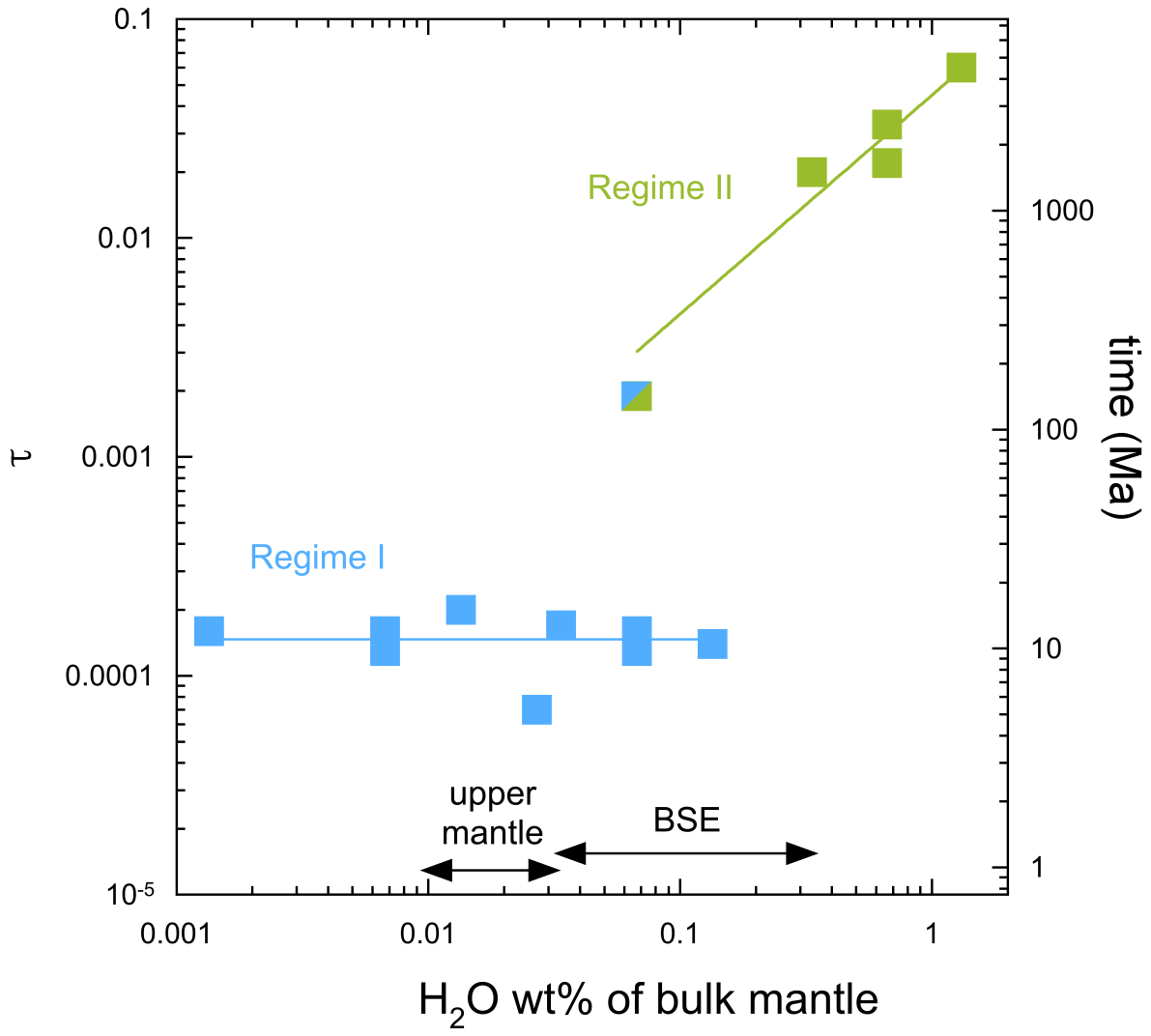

Figure 4. Geodynamical models are similar to present-day Earth regime (I) at low water content with dimensionless recycling time τ of the hydrated crust similar to that of the reference models (τ~0.00015). Models in regime II at high water content show a linear relationship between the time of recycling and the thickness of the hydrated crust converted as a percentage of H_2O in the mantle. The thick and buoyant serpentinized crust can survive as long as one Gyr for the early Earth for the highest values of geochemical estimates of water content for the bulk silicate Earth (BSE). Scaled times are shown on the right vertical axis.

373 Table 1. Model parameters.

Parameter	Symbol	Non-dimensional value	Dimensional value
Rayleigh number	Ra	10^6	
Initial quantity of heat	Rh	20	3.7×10^{-12} W kg^{-1}
Basal temperature of the upper boundary layer (temps=0)	T_{BL}	0.72	1900 K
Temperature difference (Bottom –Top)	ΔT	1	2639 K
Reference density	ρ_m	1	4400 $kg.m^{-3}$
Thermal expansivity	α	1	4.5×10^{-5} K^{-1}
Thermal diffusivity	κ	1	10^{-6} m2.s-1
Thermal conductivity		1	4 $W.m^{-1}.K^{-1}$
Reference viscosity	η_m	1	10^{23} Pa.s
Viscosity jump factor at 660 km Activation energy for viscosity	 Ea	30 8	 142 $kJ.mol^{-1}$
Yield stress at the surface		10^4	118 MPa
Hydrated crust viscosity and yielding factor		0.1	
Thickness of the model Thickness of the upper boundary layer	r r_{BL}	1 0.07 – 0.09	2900 km 203 – 261 km
Thickness of the crust	r_c	0 – 0.068	0 – 200 km
Buoyancy number for the crust	B_c	-3.4 – 0	

374
375
376

377

Table 2: Inputs and outputs of the models. r_{BL} and r_c: thickness of the final top boundary layer and of the original crust, respectively. B_c and B_{bl}: initial buoyancy number of the crust. τ: characteristic recycling time.

Name	Buoyant crust	r_{BL}	r_c	B_c	τ
Ref-1	No	0.09	0.068	0	0.00010
Ref-2	No	0.09	0.017	0	0.00012
200-100-2	Yes	0.08	0.068	-3.4	∞
200-50-2	Yes	0.08	0.068	-1.7	0.06
200-5-1	Yes	0.08	0.068	-0.17	0.00014
200-1-1	Yes	0.08	0.068	-0.03	0.00007
100-100-1	Yes	0.09	0.03	-3.4	∞
100-50-1	Yes	0.09	0.03	-1.7	0.033
100-50-2*	Yes	0.09	0.03	-1.7	0.022
100-5-1	Yes	0.09	0.03	-0.17	0.00016
100-5-2*	Yes	0.09	0.03	-0.17	0.00013
100-1-1	Yes	0.09	0.03	-0.03	0.0002
50-100-3	Yes	0.09	0.017	-3.4	0.054
50-50-1	Yes	0.09	0.017	-1.7	0.02
50-5-1	Yes	0.09	0.017	-0.17	0.00017
50-1-1	Yes	0.09	0.017	-0.03	0.00016
10-100-2	Yes	0.07	0.003	-3.4	0.022
10-50-1§	Yes	0.07	0.003	-1.7	0.0019
10-5-1	Yes	0.07	0.003	-0.17	0.00013
10-1-1	Yes	0.07	0.003	-0.03	0.00016

* simulations with no rheological contrast between the hydrated crust and mantle.
§ calculation results with mixed first and second regime character.

385 Graphical abstract
386

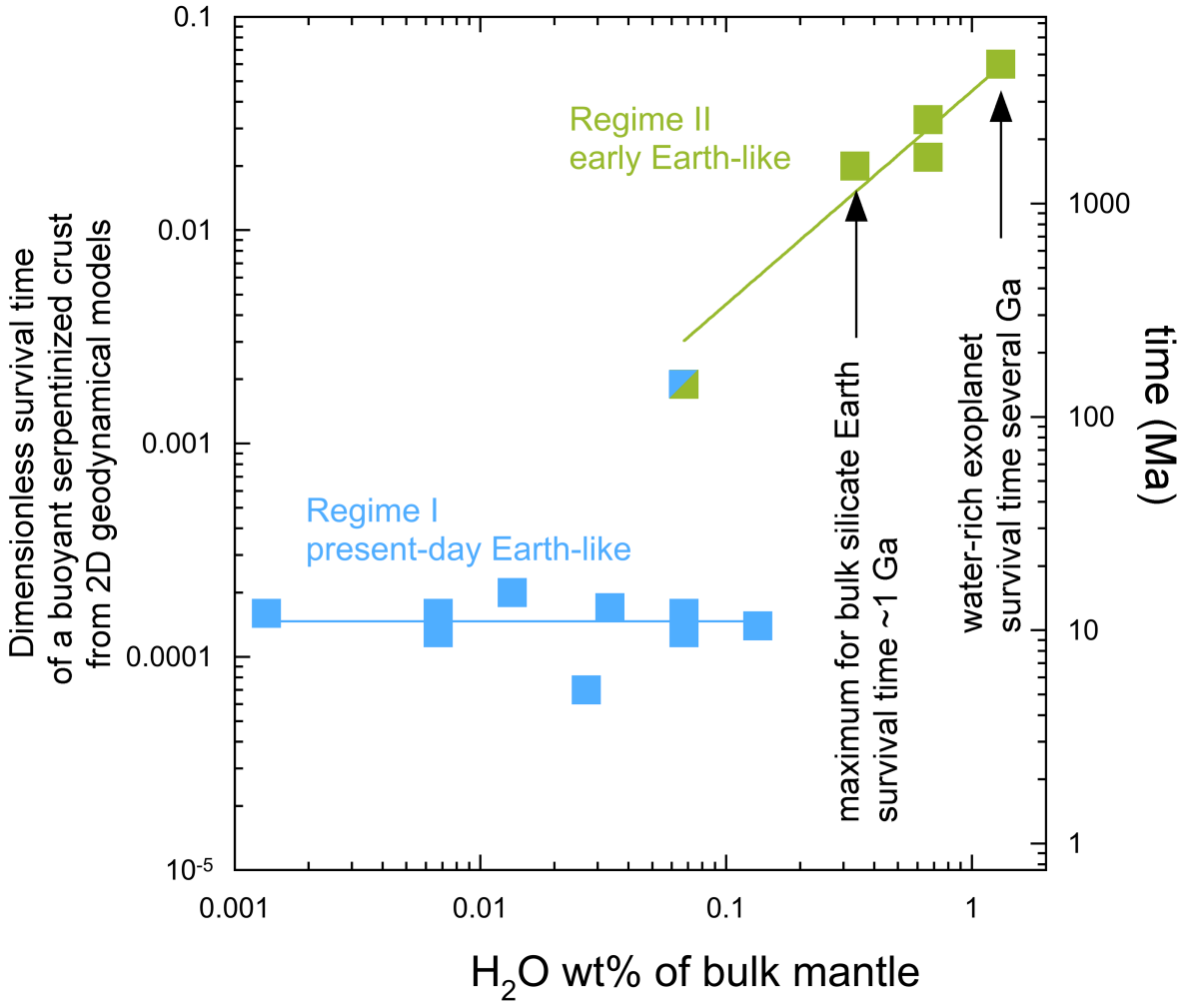

387
388